

Chapter 13

Study on Bearing Mechanism of Composite Stiffened Panel with Delamination Under Shear Load



Xue Bi, Peng Zou, and Xiangming Chen

Abstract As a typical thin wall structure, the composite stiffened panel not only has the splendid properties of composite material, but also shows the excellent performance of the composite wall structure with low quality and high bearing capacity. For the structure, the buckling and post-buckling failure of the panel and the effect of damage on the performance of the stiffened panel will happen. Thus, in this paper, the effect of damage on post-buckling bearing capacity of composite stiffened panels under shear load is researched. Three finite element models are built, including no damage shear model, delamination embedded shear model and shear after impact model. The shear failure, effect of delamination and impact damage on panel bearing strength is discussed. Furthermore, the effects of the size of delamination and position of impact on structure performance are also researched. These researches provided abundant theoretical supports for the experiment design and hopeful to be applied in industry manufacturing.

Keywords Shear load · Delamination · Stiffened panel

13.1 Introduction

Due to the excellent specific strength, specific stiffness and fatigue resistance, carbon fiber reinforced polymer (CFRP), is widely used in the aviation and aerospace industries. The composite stiffened panel, as a typical thin wall structure with low quality and high bearing capacity, plays a significant role in aircraft design because of its outstanding performance, such as fuselages, horizontal/vertical tail wings and wing. For the research on typical failure modes of composite stiffened panel, more attention should be paid to the buckling and post-buckling performance failure and damage defect. The bearing capacity of composite stiffened panel under different loads have been studied by many famous relevant institutions, such as COCOMAT [1] (Improved

X. Bi (✉) · P. Zou · X. Chen

Full Scale Aircraft Structural Static/Fatigue Laboratory, AVIC Aircraft Strength Research Institute of China, Xi'an 710065, China
e-mail: 441811017@qq.com

Material Exploitation at Safe Design of Composite Airframe Structures by Accurate Simulation of Collapse) and POSICOSS (Improved Post-buckling Simulation for Design of Fiber Composite stiffened Fuselage Structures) [2] etc.

The bearing capacity of composite stiffened panel is easily affected by low velocity impact damage that may occur during the working process of tool dropping, runway gravel and hail [3, 4]. In the impact damage, both barely visible impact damage (BVID) and visible impact damage (VID) can be encountered and cause a significant decrease in structural strength and endanger flight safety. In addition, reinforced composite materials often bear in-plane compression load and shear load during aircraft service, so relevant researchers have carried out a lot of research work on composite stiffened panels after impact [5–22]. Buckling and post buckling behavior of Glare laminates containing splices and doublers were researched from both instrumented tests [5] and numerical modelling [6]. Yu Feng et al. investigated effect of impact damage positions on the buckling and post-buckling behaviors of stiffened composite panel under compression load [7], shear load [8], fatigue load and compression-after-impact- fatigue (SAIF) load [9] and shear-after-impact- fatigue (SAIF) behaviors [10]. Sun Wei et al. [11, 12] made an experimental and finite element research on effect of stiffener damage caused by low velocity impact on compressive buckling and failure modes of T-stiffened composite panels. In addition, the edge impact damage, which shows different damage mechanism on Compression-After-Impact (CAI) behavior of stiffened composite panels, is discussed in [13]. The panel style is also a research point, except T-stiffened panel [14–16], J-stiffened panel [17–19] and hat-stiffened panel [20–22]. It is found that the research on the bearing capacity of stiffened panels after impact is mainly focused on compression load, while the research on in-plane shear load is limited, especially for the research on the influence of delamination position and size on the post buckling performance of structures, there is still a lack of targeted research work. Therefore, this paper will focus on the failure mechanism of composite stiffened panels under in-plane shear loading.

13.2 Question Description

13.2.1 Configuration and Size of Specimen

In this project, the effect of embedded damage on load-bearing failure and post buckling performance of three stringer stiffened panels under shear load is studied. Two kinds of simulation models are studied: nondestructive model and embedded delamination damage model. The type of stringer is type I. The configuration and detailed dimensions of the test piece are shown in Fig. 13.1. The configuration size and section of type I stringer are shown in Fig. 13.2. The paving of each part of the stiffened plate is shown in Table 13.1. Among them, the skin and the stringer are glued together, and the adhesive film is J-116b with a thickness of 0.2 mm.

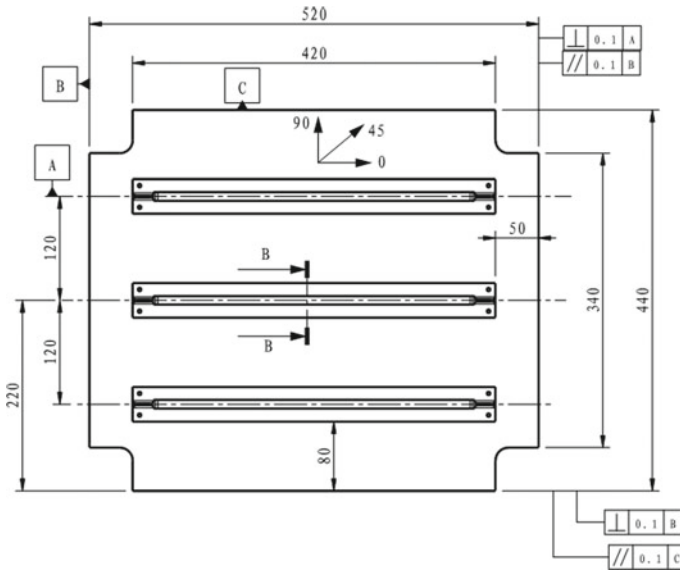


Fig. 13.1 Dimensions of shear test pieces for type I stiffened plates (mm)

13.2.2 Material System

The laminate material system is CCF300/BA9916-II, which is manufactured by conventional prepreg method. The nominal thickness of the single layer is 0.155 mm, the nominal fiber volume content is about 62%, and the porosity is within 2.0%. The material properties are shown in Table 13.2 below.

13.2.3 Size and Location of Precast Layers

This study mainly simulates the delamination prefabricated by polytetrafluoroethylene film between the truss and the skin. The position of the simulated delamination in the finite element method is shown in Fig. 13.3. The delamination dimensions are 40 × 40 mm, 80 × 40 mm and 120 × 40 mm.

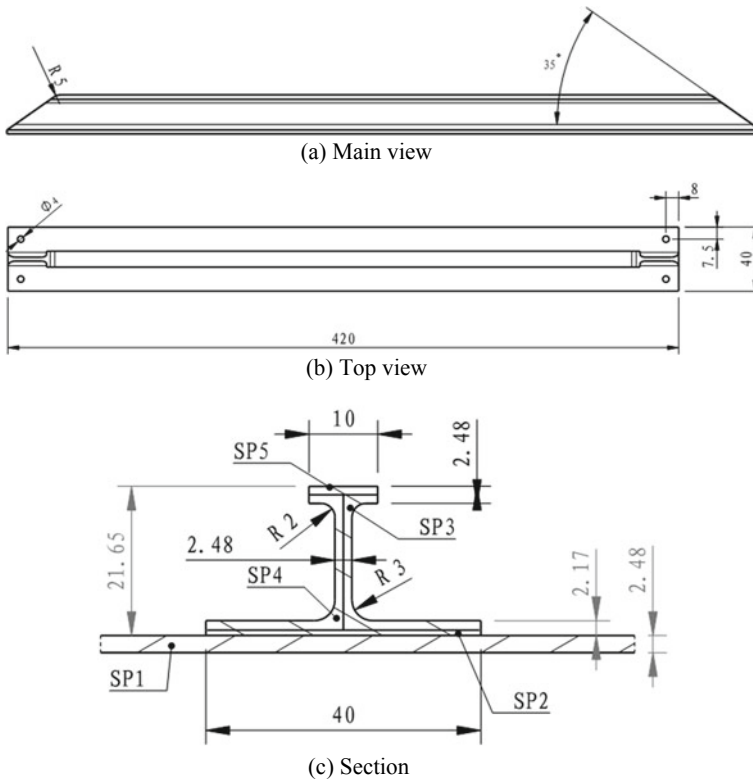


Fig. 13.2 Configuration and size of I-type stringer (mm)

13.3 Numerical Simulation Method

13.3.1 Finite Element Model

According to the specimen configuration and size in the previous section, two types of finite element models are established in this study: (a) the non-destructive shear loading model; (b) the prefabricated layered shear loading model between the truss and skin, as shown in Fig. 13.4 below.

The main components of various models are described as follows: for (a) model, it is mainly composed of skin, bottom plate of flange, flange-web-upper flange (right), flange-web-upper flange (left) and upper flange roof, which is mainly composed of traditional deformable shell elements. Meanwhile, in order to keep the basic conditions of the other two models consistent, and to compare and analyze the effects of damage and delamination on the post buckling capacity under shear load, cohesive elements are preset between 1–2, 8–9 and 15–16 layers of the skin, and between the skin and the bottom flange plate. In model (b), based on model (a), the corresponding

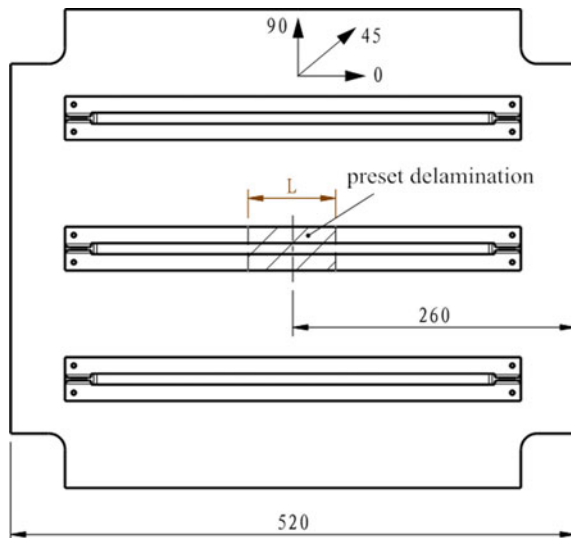
Table 13.1 Laying sequence of each part of stiffened plate

Ply code	Position	Ply ratio (0/ ± 45/90)	Laying sequence	Number of layers	Nominal thickness [mm]
SP1	Skin	(37.5/50/12.5)	[45/-45/0/45/90/0/-45/0] _S	16	2.48
SP2	Bottom plate of flange	(33/50/17)	[0/45/90/0/-45/45]	6	0.93
SP3	Flange, web and upper flange (right)	(37.5/50/12.5)	[0/-45/0/90/45/0/-45/45]	8	1.24
SP4	Flange, web and upper flange (left)	(37.5/50/12.5)	[0/45/0/90/-45/0/45/-45]	8	1.24
SP5	Upper flange roof	(37.5/50/12.5)	[0/-45/0/90/45/0/-45/45]	8	1.24

Table 13.2 CCF300/BA9916-II, unidirectional board performance

E ₁ [Gpa]	E ₂ [Gpa]	G ₁₂ [Gpa]	ν ₁₂	X ^T [Mpa]	X ^C [Mpa]	Y ^T [Mpa]	Y ^C [Mpa]	S [Mpa]
124.8	9.755	5.26	0.312	1871	1291	59.7	215	102

Fig. 13.3 Location of preset delamination of shear test piece of type I stiffened plate (mm)



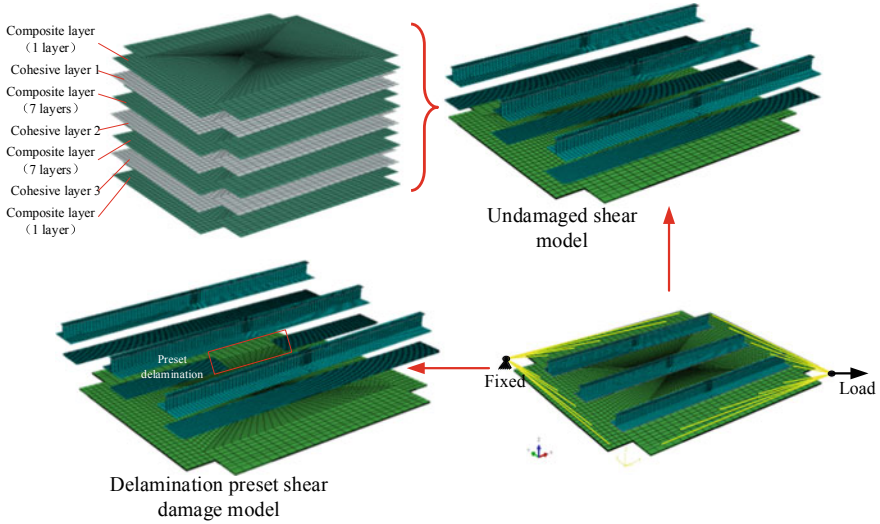


Fig. 13.4 Finite element model

delamination size is preset between the bottom plate of the flange and the skin of the middle stringer, that is, the cohesive element layer is divided into corresponding space. The load and boundary conditions for both models are set as follows: two adjacent sides of the panel are coupled to the reference point, which is set fixed. The other two adjacent sides are also coupled to another reference point, where a displacement load is applied. In addition, the four sides are restrained in the direction perpendicular to the panel. Detailed boundary conditions are shown in Fig. 13.4.

13.3.2 Constitutive Model

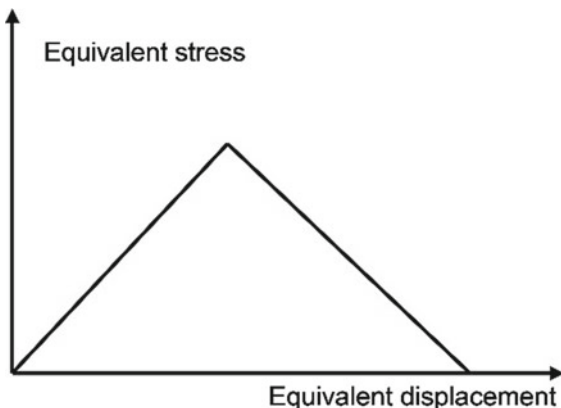
For the prediction of the in-plane damage of composite laminates, the Hashin failure criterion of ABAQUS is used to judge the initial failure of in-plane damage. The discriminant formulas of various failure forms are provided in Eqs. (13.1)–(13.4):

$$\text{Fiber tensile failure : } F_f^t = \left(\frac{\sigma_{11}}{X^T} \right)^2 + \alpha \left(\frac{\tau_{12}}{S^L} \right)^2 \sigma_{11} \geq 0 \quad (13.1)$$

$$\text{Fiber compression failure : } F_f^c = \left(\frac{\sigma_{11}}{X^C} \right)^2 \sigma_{11} < 0 \quad (13.2)$$

$$\text{Tensile failure of matrix : } F_m^t = \left(\frac{\sigma_{22}}{Y^T} \right)^2 + \left(\frac{\tau_{12}}{S^L} \right)^2 \sigma_{22} \geq 0 \quad (13.3)$$

Fig. 13.5 Linear damage evolution constitutive model



Compression failure of matrix :

$$F_m^c = \left(\frac{\sigma_{22}}{2S^T}\right)^2 + \left[\left(\frac{Y^C}{2S^T}\right)^2 - 1\right] \frac{\sigma_{22}}{Y^C} + \left(\frac{\tau_{12}}{S^L}\right)^2 \sigma_{22} < 0 \tag{13.4}$$

The linear degradation criterion based on energy is used for damage evolution, and the final failure condition of the element is determined by inputting the energy requirements under various failure modes (the area of the triangle in Fig. 13.5 below).

The bilinear constitutive model based on cohesive element is used to predict the delamination damage of composite laminates. The constitutive equation of the interface represents the mechanical relationship between the interfacial traction force and the relative separation displacement of the interface, and the curve of the traction separation constitutive relationship is shown in Fig. 13.6.

Figure 13.6a describes the normal behavior of the interface, Fig. 13.6b describes the behavior of two tangent directions of the interface, and Fig. 13.6c is a bilinear constitutive model of mixed mode under the combined action of tensile delamination and shear delamination. The mixed pattern in Fig. 13.6c graph is the key to express the hierarchical coupling, and its corresponding initiation and expansion criteria also change. ABAQUS provides an elastic relationship that directly defines traction and separation, which can be expressed as Eq. (13.5):

$$\begin{Bmatrix} t_n \\ t_s \\ t_t \end{Bmatrix} = \begin{bmatrix} K_n & & \\ & K_s & \\ & & K_t \end{bmatrix} \begin{Bmatrix} \delta_n \\ \delta_s \\ \delta_t \end{Bmatrix} \tag{13.5}$$

- t_n, t_s and t_t : nominal traction in normal and two tangential directions;
- δ_n, δ_s and δ_t : corresponding displacement value;
- K_n, K_s and K_t : respective interface stiffness.
- $K_i (i = n, s, t)$ can be expressed by Eq. (13.6):

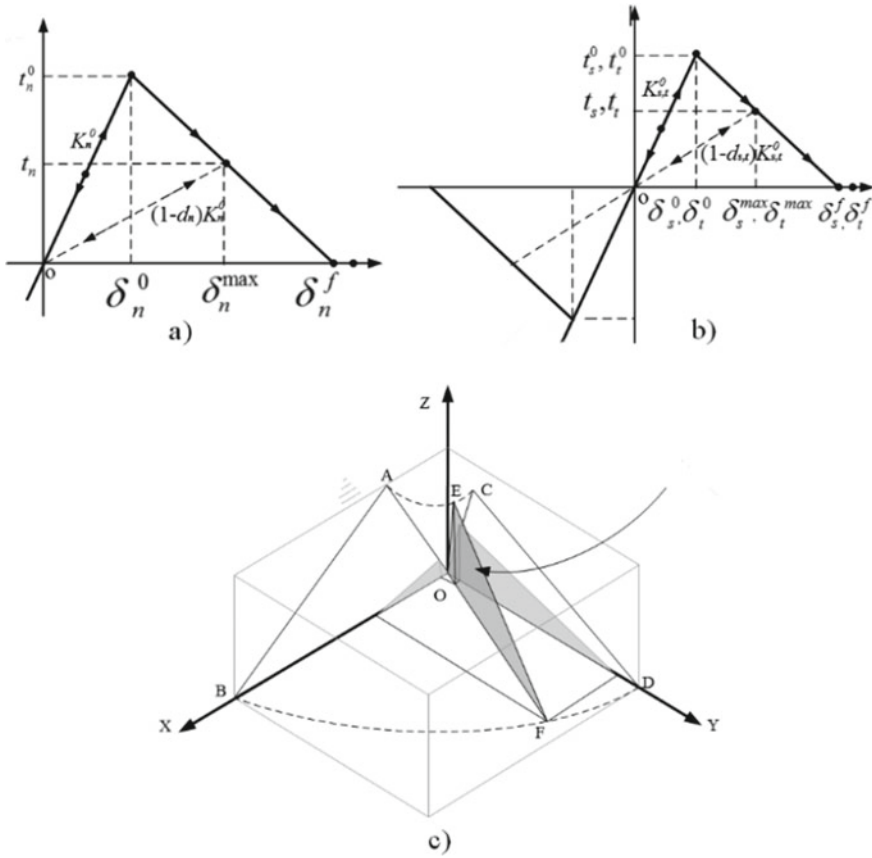


Fig. 13.6 Cohesive bilinear constitutive model: **a** normal behavior, **b** tangential behavior, **c** mode mixing

$$K_i = \begin{cases} K_i^0 & \delta_i \leq \delta_i^0 \\ (1 - d_i)K_i^0 & \delta_i^0 \leq \delta_i \leq \delta_i^f \\ 0 & \delta_i \geq \delta_i^f \end{cases} \quad i = n, s, t \quad (13.6)$$

K_i^0 : initial stiffness of interface;

δ_i^0 and δ_i^f : in single mode, the nominal strain values when stratified initiation and stratification are completely formed.

d_i : damage variables that controlling delamination propagation expansion.

After the initiation of delamination, the delamination behavior of the interface layer is controlled by the delamination softening law. The secondary nominal stress criterion is used to predict the initiation of mixed mode delamination, as shown in the following formula, which allows each traction component to interact to produce

Table 13.3 Cohesion model parameters

Parameters	Value
Mode I delamination critical strain energy release rate [mJ/mm ²]	0.434
Mode delamination critical strain energy release rate [mJ/mm ²]	0.744
Mode delamination critical strain energy release rate [mJ/mm ²]	0.744
Interface strength $t_{0n}/t_s^0/t_t^0$ [MPa]	20/35/35
Initial interface stiffness K [N/mm ³]	5000/1923/1923

delamination together. When the traction stress rate meets the following criteria (Eq. (13.7)), delamination begins.

$$\left\{ \frac{\langle t_n \rangle}{t_n^0} \right\}^2 + \left\{ \frac{t_s}{t_s^0} \right\}^2 + \left\{ \frac{t_t}{t_t^0} \right\}^2 = 1 \quad (13.7)$$

Hierarchical expansion criterion is used to judge the occurrence of delamination. In this paper, energy based hierarchical evolution method is adopted. At present, there are two energy criteria: energy law criterion and B-K criterion. In combination with relevant research literature, this paper uses energy law to define mixed mode delamination failure, as shown in the Eq. (13.8):

$$\left[\frac{G_n}{G_n^C} \right]^\beta + \left[\frac{G_s}{G_s^C} \right]^\beta + \left[\frac{G_t}{G_t^C} \right]^\beta = 1 \quad (13.8)$$

G_s and G_t : instantaneous fracture energy in three directions;

G_n^C , G_s^C and G_t^C : critical fracture energy causing normal and two tangential delamination in single mode.

β : empirical parameters, it is used to characterize the coupling degree of the three layered modes, and the value of β in this paper is taken as 1.

The material properties used in the simulation are shown in Table 13.3.

13.4 Shear Failure Analysis of Intact Stiffened Panel

13.4.1 Skin Damage Analysis

Figure 13.7 shows the location of the initial delamination damage. It can be seen from Fig. 13.7 that the initial delamination of intact stiffened panels mainly occurs on the bottom skin of the lower flange of the middle stringer. Three cohesive layers are set up in the simulation, the stratification degree of each layer is basically the

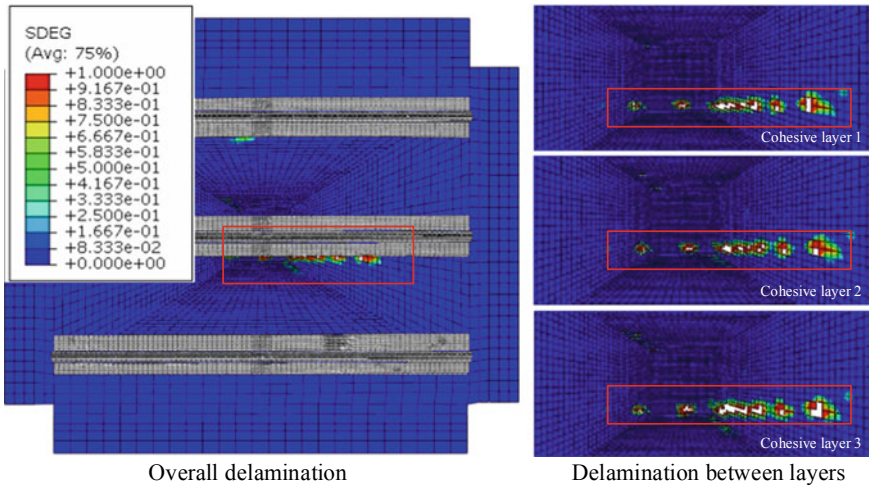


Fig. 13.7 Analysis of initial delamination position of skin

same, and the stratification degree of upper and lower layers is slightly larger than that of the middle layer, which is mainly related to the deformation degree of different delamination positions along the thickness direction. Because of being close to the loading end, the skin of the upper stringer also has a certain tendency of delamination, while there is no delamination at the lowest stringer near the fixed end.

With the load increases, the delamination will extend vertically and horizontally. It can be seen from Fig. 13.8 that the delamination will gradually expand along the longitudinal axis of the middle stringer after the delamination occurs at the bottom of the flange under the middle stringer, but it is difficult to extend to the other two stringers, which is different from the case of stringer debonding in the following paper. In addition, the law is consistent in the three-layer cohesive unit

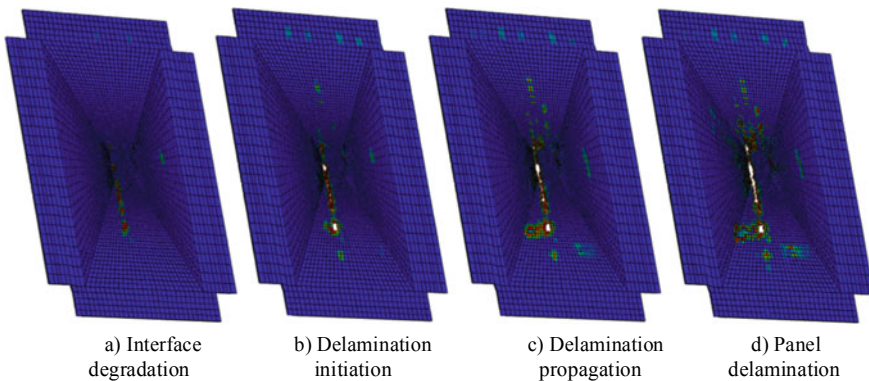


Fig. 13.8 Analysis of delamination growth

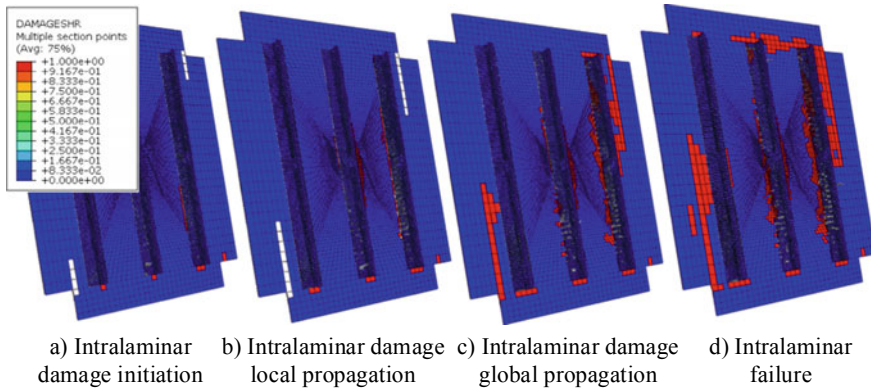


Fig. 13.9 Damage analysis in skin layer

layer, indicating that the ply angle near the ply has little effect on the delamination propagation.

Figure 13.9 shows the in-plane damage of the skin. The in-plane damage first occurs at the bottom edge of the lower flange of the truss near the loading end, and the damage is mainly based on the matrix tension, and there is no other form of damage. This is mainly due to the lower properties of matrix and fiber.

At the moment, slight matrix damage will not affect the bearing capacity of the structure, and the bearing capacity is still in the rising stage. With the increase of load, the damage extends under the three stringers, especially at the lower flange of the two stringers near the loading point, and there are also a lot of damage at the edge of the skin, which is mainly caused by the boundary constraints in the simulation process, which may be different from the actual test.

13.4.2 Analysis of Skin-Flange Debonding

Figure 13.10 shows the debonding of the stringer during the loading process. It can be seen from the figure that the debonding starts at the stringer near the loading end

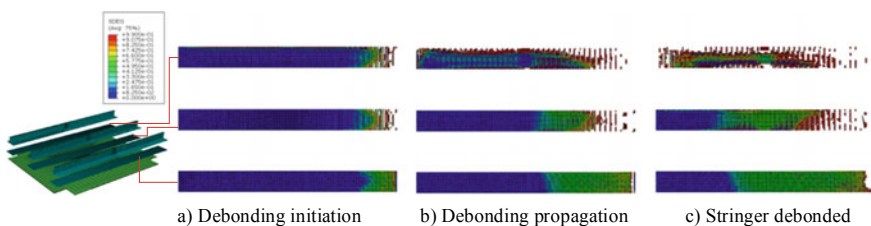


Fig. 13.10 Analysis on debonding of flange

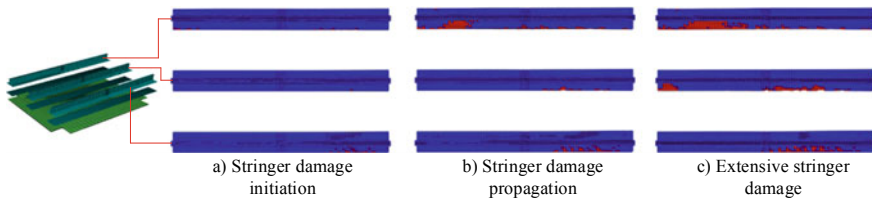


Fig. 13.11 Damage propagation analysis of stringer

and gradually expands inward along the diagonal line. Meanwhile, with the increase of load, debonding also occurs at the other two stringers.

13.4.3 Damage Analysis of Stringer

Figure 13.11 shows the damage propagation of the stringer. It can be seen from the figure that the damage first occurs on the stringer near the loading point, and then the three stringers have different degrees of in-plane damage, and mainly distributed in the lower half of the lower flange. Compared with skin damage and skin-stringer debonding damage, it can be concluded that due to the relatively low property setting of adhesive film in the simulation process, the premature debonding between the skin and the stringer reduces the load transferred to the stringer. Therefore, the damage of the stringer is relatively light under the condition of large area damage of the skin under three stringers.

13.5 Analysis of the Influence of Embedded Delamination on Shear Failure

13.5.1 Analysis of the Influence of Embedded Delamination on Skin

In this study, three kinds of delamination sizes, 40 mm × 40 mm, 80 mm × 40 mm and 120 mm × 40 mm, are taken into account. Figures 13.12 and 13.13 show the in-plane damage and delamination damage propagation under different sizes of embedded defects, and it can be seen from the figure that for in-plane damage, the influence of embedded defects with different sizes on in-plane damage at each stage is very small. Compared with the delamination damage at the same stage (corresponding to the last stage of in-plane damage propagation), the delamination damage of 80 mm × 40 mm embedded defects is relatively larger, while that of 120 mm × 40 mm is the

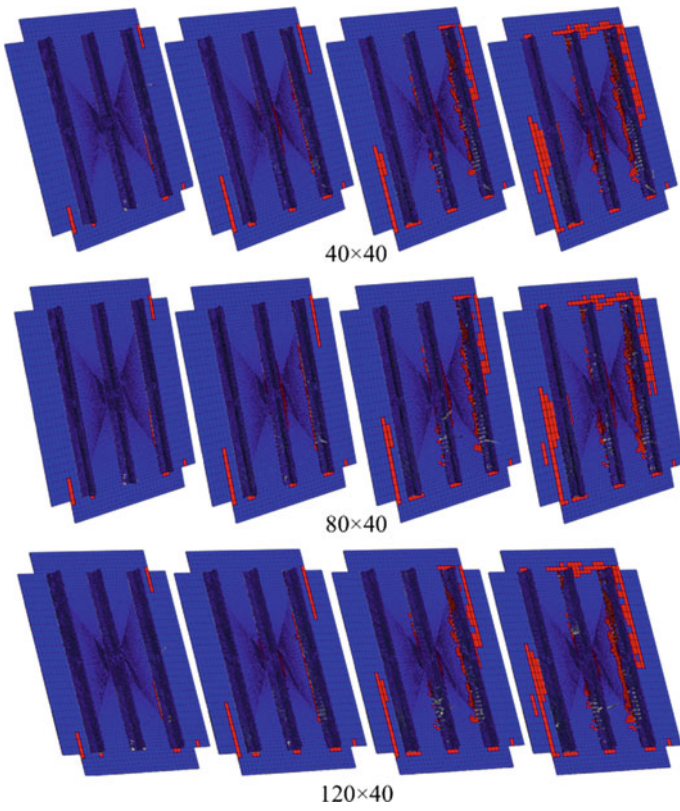


Fig. 13.12 Effect of embedded delamination on in-plane damage of skin

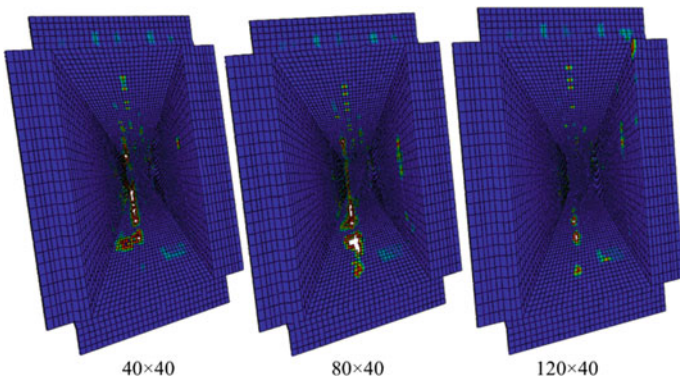


Fig. 13.13 Effect of embedded delamination on skin delamination damage

smallest. In general, the size of delamination damage is smaller than that of in-plane damage (mainly in-plane matrix damage).

13.5.2 Analysis of the Influence of Embedded Delamination on Skin-Stringer Debonding

Figure 13.14 shows the effect of different size embedded defects on skin-stringer debonding. It can be studied that the delamination propagation law is basically consistent. For the middle truss with embedded defects, delamination mainly extends from the right half to the left, and the left side begins to gradually occur when the right side is almost completely layered.

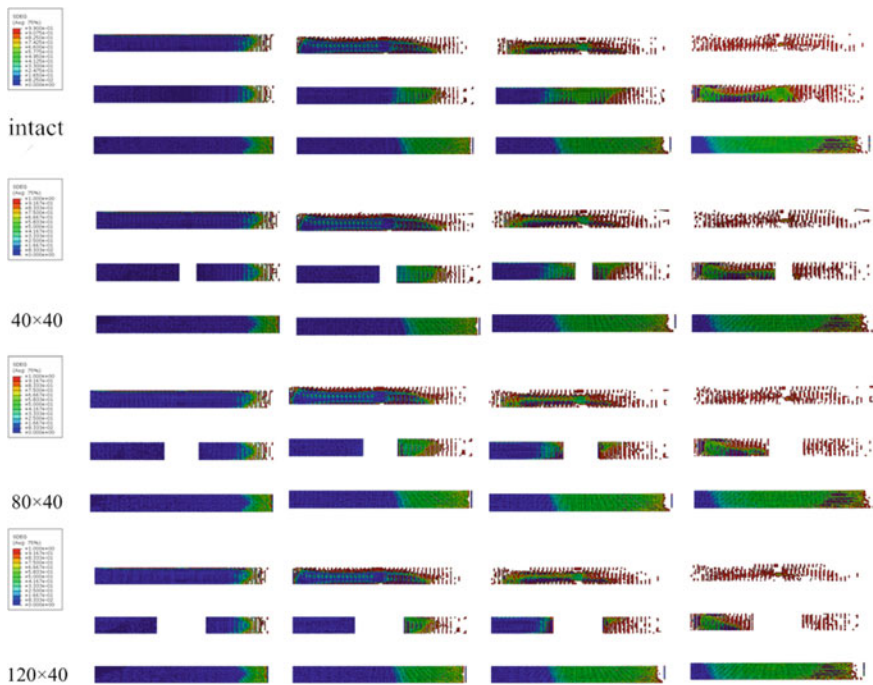


Fig. 13.14 Effect of embedded delamination on skin-stringer debonding

13.5.3 Analysis of the Influence of Embedded Delamination on the Damage of Stringer

Similarly, due to the relatively weak performance of the adhesive film, the premature debonding between the skin and the stringer reduces the load transferred to the stringer. Therefore, the influence of different sizes of embedded delamination on the damage propagation law of the stringer is also weak. It can be seen from Fig. 13.15 below that there is no obvious difference in the damage degree and distribution of the stringer.

From the above analysis, it can be seen that different sizes of embedded delamination have limited influence on the damage propagation of skin and stringer. The main reason is that the performance of the adhesive film is relatively weak. Before the damage of the skin and the stringer, they will be debonding prematurely, which reduces the load transferred to the stringer.

Taking the embedded delamination of $80\text{ mm} \times 40\text{ mm}$ as an example, the damage propagation of each part is shown in Fig. 13.16 below. It can be found that there is a large degree of debonding when the in-plane initial damage occurs to the skin,

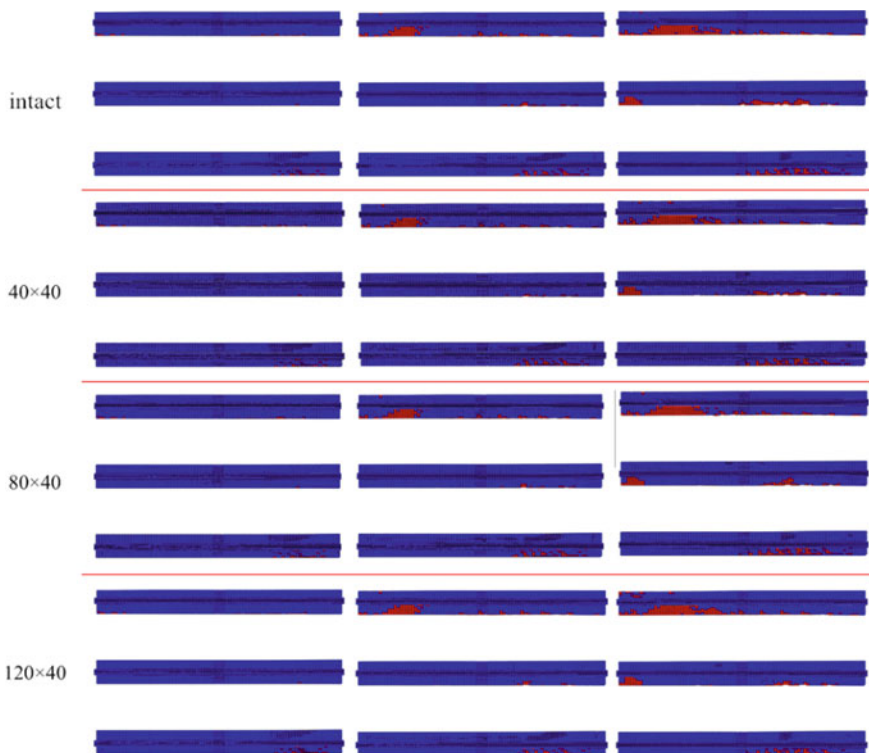


Fig. 13.15 Effect of embedded delamination on damage of stringer

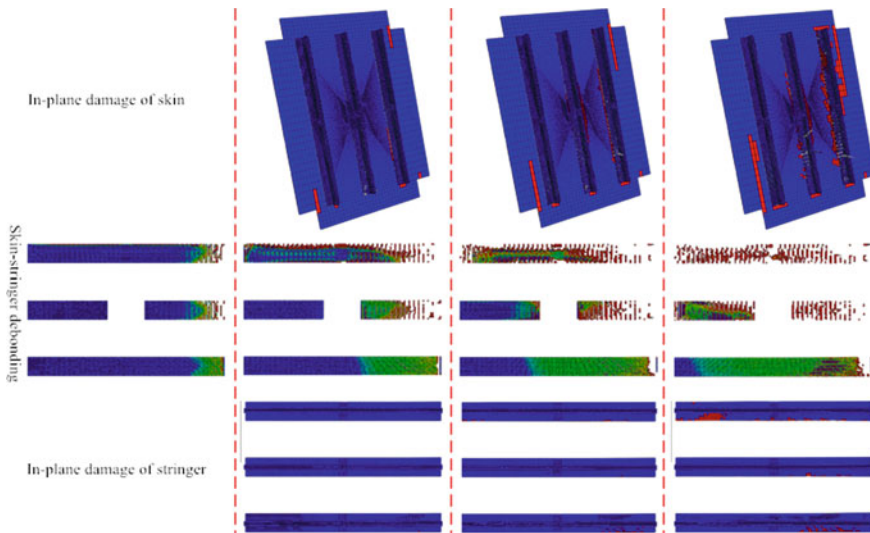


Fig. 13.16. Damage extension

while the stringer is not damaged at this time. When the damage occurs, the degree of debonding is more serious. As a result, both skin and stringer are less affected by the size of embedded layer.

13.6 Conclusions

In this report, the influence of defect damage on the post buckling capacity of composite stiffened panels under shear loading is studied. The damage free shear model and the prefabricated delamination damage shear model are established. The influence of the damage of the prefabricated delamination between the skin and the truss on the mechanical properties of the stiffened panel under shear load is analyzed, and the influence of the size of the prefabricated delamination on the results is further studied, which provides theoretical support for the experimental design. The main conclusions are as follows:

- (a) For intact stiffened panels, the initial delamination occurs at the skin of the bottom flange of the middle stringer, and the in-plane damage first occurs at the bottom skin of the lower flange of the stringer near the loading end, and the damage is mainly caused by matrix tension. The results show that the debonding starts from the stringer near the loading end and gradually expands inward along the diagonal line. The damage of the stringer occurs on the stringer close to the loading point, and then the three stringers have different degrees of in-plane

damage, and mainly distributed in the position where the lower flange is far away from the loading point.

- (b) The main reason of different size of embedded delamination on the damage propagation of skin and stringer is limited is that the performance of the adhesive film is relatively low, and the debonding of the skin and the stringer occurs prematurely before the damage occurs, which reduces the load transferred to the stringer.

References

1. Degenhardt, R., Rolfes, R., Zimmermann, R., Rohwer, K.: COCOMAT—improved material exploitation of composite airframe structures by accurate simulation of postbuckling and collapse. *Compos. Struct.* **73**(2), 175–178 (2006)
2. Zimmermann, R., Rolfes, R.: POSICOSS—improved postbuckling simulation for design of fibre composite stiffened fuselage structures. *Compos. Struct.* **73**(2), 171–174 (2006)
3. Mcelroy, M.: Use of an enriched shell finite element to simulate delamination-migration in a composite laminate. *Compos. Struct.* **167**, 88–95 (2017)
4. Park, H., Kong, C.: Experimental study on barely visible impact damage and visible impact damage for repair of small aircraft composite structure. *Aerosp. Sci. Technol.* **29**, 363–372 (2013)
5. Al-Azzawi, A.S.M., McCrory, J., Kawashita, L.F., Featherston, C.A., Pullin, R., Holford, K.M.: Buckling and postbuckling behaviour of Glare laminates containing splices and doublers. Part 1: Instrumented tests. *Compos. Struct.* **176**, 1158–1169 (2017)
6. Al-Azzawi, A.S.M., Kawashita, L.F., Featherston, C.A.: Buckling and postbuckling behaviour of Glare laminates containing splices and doublers. Part 2: Numerical modelling. *Compos. Struct.* **176**, 1170–1187 (2017)
7. Feng, Y., Zhang, H., Tan, X., He, Y., An, T., Zheng, J.: Effect of impact damage positions on the buckling and post-buckling behaviors of stiffened composite panel. *Compos. Struct.* **155**, 184–196 (2016)
8. Feng, Y., He, Y., Tan, X., An, T., Zheng, J.: Experimental investigation on different positional impact damages and shear-after-impact (SAI) behaviors of stiffened composite panels. *Compos. Struct.* **178**, 232–245 (2017)
9. Feng, Y., He, Y., Zhang, H., Tan, X., An, T., Zheng, J.: Effect of fatigue loading on impact damage and buckling/post-buckling behaviors of stiffened composite panels under axial compression. *Compos. Struct.* **164**, 248–262 (2017)
10. Feng, Y., He, Y., Tan, X., An, T., Zheng, J.: Investigation on impact damage evolution under fatigue load and shear-after-impact-fatigue (SAIF) behaviors of stiffened composite panels. *Int. J. Fatigue* **100**, 308–321 (2017)
11. Sun, W., Guan, Z., Ouyang, T., Tan, R., Zhong, X.: Effect of stiffener damage caused by low velocity impact on compressive buckling and failure modes of T-stiffened composite panels. *Compos. Struct.* **184**, 198–210 (2018)
12. Sun, W., Guan, Z., Li, Z., Ouyang, T., Jiang, Y.: Modelling and simulating of the compressive behavior of T-stiffened composite panels subjected to stiffener impact. *Compos. Struct.* **186**, 221–232 (2018)
13. Li, N., Chen, P.: Experimental investigation on edge impact damage and Compression-After-Impact (CAI) behavior of stiffened composite panels. *Compos. Struct.* **138**, 134–150 (2016)
14. Boni, L., Fanteria, D., Lanciotti, A.: Post-buckling behaviour of flat stiffened composite panels: Experiments vs. analysis. *Compos. Struct.* **94**(12), 3421–3433 (2012)

15. Wang, X., Cao, W., Deng, C., Wang, P., Yue, Z.: Experimental and numerical analysis for the post-buckling behavior of stiffened composite panels with impact damage. *Compos. Struct.* **133**, 840–846 (2015)
16. Masood, S.N., Vishakh, R., Viswamurthy, S.R., Gaddikeri, K.M., Sridhar, I.: Influence of stiffener configuration on post-buckled response of composite panels with impact damages. *Compos. Struct.* **194**, 433–444 (2018)
17. Bai, R., Lei, Z., Wei, X., Tao, W., Yan, C.: Numerical and experimental study of dynamic buckling behavior of a J-stiffened composite panel under in-plane shear. *Compos. Struct.* **166**, 96–103 (2017)
18. Lei, Z., Bai, R., Tao, W., Wei, X., Leng, R.: Optical measurement on dynamic buckling behavior of stiffened composite panels under in-plane shear. *Opt. Lasers Eng.* **87**, 111–119 (2016)
19. Chen, Q., Qiao, P.: Post-buckling analysis of composite plates under combined compression and shear loading using finite strip method. *Finite Elem. Anal. Des.* **83**, 33–42 (2014)
20. Raju, G., Wu, Z., Weaver, P.M.: Buckling and postbuckling of variable angle tow composite plates under in-plane shear loading. *Int. J. Solids Struct.* **58**, 270–287 (2015)
21. Zhang, T., Li, S., Chang, F., Shi, X., Li, L.: An experimental and numerical analysis for stiffened composite panel subjected to shear loading in hygrothermal environment. *Compos. Struct.* **138**, 107–115 (2016)
22. Tsai, S.W.: *Composite design*, 4th edn. Think Composites, Dayton (1988)